GEOPHYSICS, VOL. 82, NO. 2 (MARCH-APRIL 2017); P. C35–C47, 12 FIGS.
10.1190/GEO2016-0191.1

Efficient wave-mode separation in vertical transversely isotropic media

Yang Zhou[1] and Huazhong Wang[1]

ABSTRACT

Wave-mode separation can be achieved by projecting elastic wavefields onto mutually orthogonal polarization directions. In isotropic media, because the P-wave's polarization vectors are consistent with wave vectors, the isotropic separation operators are represented by divergence and curl operators, which are easy to realize. In anisotropic media, polarization vectors deviate from wave vectors based on local anisotropic strength and separation operators lose their simplicity. Conventionally, anisotropic wave-mode separation is implemented either by direct filtering in the wavenumber domain or nonstationary filtering in the space domain, which are computationally expensive. Moreover, in conventional anisotropic separation, correcting for amplitude and phase changes of waveforms by applying separation operators is also more difficult than in an isotropic case. We have developed new operators for efficient wave-mode separation in vertical transversely isotropic (VTI) media. Our separation operators are constructed by local rotation of wave vectors to directions where the quasi-P (qP) wave is polarized. The deviation angles between the wave vectors and the qP-wave's polarization vectors are explicitly estimated using the Poynting vectors. Obtaining polarization directions by rotating wave vectors yields separation operators in VTI media with the same forms as divergence and curl operators, except that the spatial derivatives are now rotated to implement wavefield projections in accurate polarization directions. The main increase in computational cost relative to isotropic separation operators is the estimation of the Poynting vectors, which is relatively small within elastic-wave extrapolation. As a result, applying the proposed operators is efficient. In the meantime, the waveforms corrections for divergence and curl operators can be directly extended for our new operators due to the similarities between these operators. By numerical exercises, we have determined that wave modes can be well-separated with small numerical cost using the present separation operators. The conservation of energy in wave-mode separation by applying waveform corrections was also verified.

INTRODUCTION

Seismic wave propagation in earth material described by the elastic-wave equation is a better approximation than by the acoustic-wave equation. Seismic migration techniques based on full-elastic wavefields generally provide more information for parameter estimation and reservoir characterization. Moreover, elastic-wave migration becomes necessary even for structural imaging in some particular areas, such as a gas-cloud zone in which the P-wave energy is attenuated. However, applying the crosscorrelation imaging condition directly to extrapolated elastic wavefields generates artifacts caused by crosstalk between coupled wave modes coinciding in space and time (Yan and Sava, 2008). To obtain an uncontaminated image, wave-mode separation is required before applying the imaging condition to elastic-wave migration.

One of the most effective ways to implement wave-mode separation is by projecting elastic wavefields onto directions in which each wave mode is polarized. The projections for wave mode separation can be easily implemented to the wavenumber domain through the dot product of wavefields and polarization vectors (Dellinger and Etgen, 1990). However, applying projections in the wavenumber domain requires Fourier transforms at each time step during elastic-wave extrapolation, which is time consuming in practice. To improve computational efficiency, the projections can also be performed in the space domain. In isotropic media because the P-wave is polarized in the same directions as the wave vectors, the isotropic separation operators for implementing projections become divergence and curl operators (Dellinger and Etgen, 1990). The divergence and curl operators are cheap to realize and have been applied to elastic-wave

Manuscript received by the Editor 11 April 2016; revised manuscript received 30 August 2016; published online 20 December 2016.
[1]Tongji University, Wave Phenomenon and Inversion Imaging group, School of Ocean and Earth Science, Shanghai, China. E-mail: geo_zy@outlook.com; herbhuak@vip.163.com.

migration in isotropic media (Sun et al., 2006; Yan and Sava, 2008).

In anisotropic media, polarization directions for quasi-P (qP) and quasi-S (qS) wave modes vary from wave vectors' parallel and perpendicular directions based on the local anisotropic strength. Actually, polarization vectors now become complex functions of the wave vectors and medium parameters (Rommel, 1994). As a result, the separation operators form spatial filters that behave as isotropic separation operators with "tails" extending out in the space domain (Dellinger and Etgen, 1990). Yan and Sava (2009b) suggest the use of such spatial filters to construct separation operators in vertical transversely isotropic (VTI) media. The spatial filters are compact in the space domain so that they can adapt to media heterogeneity (Yan and Sava, 2009b). However, Yan and Sava (2011) show that point-wise implementation of such local spatial filters is computationally expensive and almost prohibitive in 3D application. To improve computational efficiency, they suggest approximating the heterogeneous model with several weighted homogeneous reference models. First, the separations are applied to each reference model in the pointwise wavenumber domain, after being transformed back to the pointwise space domain, the separated wavefields on each reference model are then interpolated to produce wavefields in the pointwise original heterogeneous model. This scheme is a trade-off between efficiency and accuracy; thus, choosing the number of reference models is model-dependent, and so is the computational cost. An alternative approach to derive efficient wave-mode separation in anisotropic media is proposed by Cheng and Fomel (2014). They suggest rewriting the projection relations between wavefields and polarization vectors as space-wavenumber domain integral operations, then numerically solve the operators by low-rank approximation. The low-rank approximation reduces the numerical cost of solving the original integral operations by representing the whole model positions and wavenumber ranges with a few selective ones, the number of which is significantly reduced when compared with the original model and wavenumber spaces. As pointed out in their paper, the computational cost of this algorithm increases with the model size and the complexity of model. As a result, in a 3D model with high heterogeneity, the computational time of this algorithm can be large.

To obtain seismic images with proper physical meanings, the amplitude and phase changes of waveforms caused by applying separation operators should be corrected. In isotropic media, by substituting a plane-wave trial solution into the divergence and curl operators, Sun et al. (2001) conclude that a $\pi/2$ phase shift is induced in separating the P- and S-waves. They further indicate that the amplitude change factor due to applying the divergence and curl operators consists of phase velocity and frequency components (Sun et al., 2011). Duan and Sava (2015) analyze the waveform changes by rewriting the spatial derivatives involved in separation operators using dispersion relationship in the wavenumber domain. They propose corrections for such distortions by integrating the source wavelet over time, followed by multiplying the extrapolated wavefields with the phase velocity corresponding to the P- and S-waves. In anisotropic media, due to the separation operators' dependencies of the local parameters, waveform changes become more complex, and no similar corrections are derived as in the isotropic case under the conventional anisotropic separation framework.

In this paper, we propose efficient wave-mode separation operators in anisotropic media. These operators are derived by locally rotating wave vectors to directions where the qP-wave is polarized, together with the orthogonality of polarization directions between the qP- and qS-waves. The deviation angles between the wave vectors and the qP-wave's polarization vectors are spatially estimated using the Poynting vectors. Under such derivation, the proposed operators become linear combinations of rotated spatial derivatives in the space domain, which can be efficiently calculated. Because the proposed operators have forms similar to the divergence and curl operators, corrections of waveform changes in isotropic media can be easily adopted in the proposed operators. We begin by giving a brief review of conventional schemes for projection-based wave-mode separation in isotropic and anisotropic media; then, detailed derivations and analyses for our new operators are given. Finally, we verify the efficiency and effectiveness of the present operators by numerical examples with 2D VTI synthetic data.

PROJECTION-BASED WAVE-MODE SEPARATION

A vector wavefield $\mathbf{U}$ can be separated into different wave modes by projecting wavefields according to the wave modes' polarization directions (Dellinger and Etgen, 1990). In 2D anisotropic media, the projection for obtaining a qP-wave has the following form (Yan and Sava, 2009b):

$$q\tilde{P} = i\mathbf{P_{qP}} \cdot \tilde{\mathbf{U}}, \tag{1}$$

where $\mathbf{P_{qP}}$ is the polarization vector for the qP-wave in the wavenumber domain and $\tilde{\mathbf{U}}$ and $q\tilde{P}$ are the wavefield variables in the Fourier domain corresponding to the elastic vector wavefield and extracted qP-wave, respectively. Using the orthogonality of the polarization directions between the qP- and qS-waves, similar expressions for qS-wave components can be obtained (Yan and Sava, 2009a). In isotropic media because the directions of the polarization vector $\mathbf{P_{qP}}$ are consistent with the directions of the wave vector $\mathbf{k}$, separation operators for implementing wavefields projections can be simplified as divergence and curl operators in the space domain (Dellinger and Etgen, 1990). The divergence and curl operators are independent of the medium parameters and only involve spatial derivatives; thus, the numerical cost of calculating these operators is small.

However, in anisotropic media, $\mathbf{P_{qP}}$ is dependent on the medium parameters, and the directions of $\mathbf{P_{qP}}$ deviate from the wave vectors' directions based on the local anisotropic strength (Thomsen, 1986). In the space domain, $\mathbf{P_{qP}}$ behaves as spatial filters instead of as simple spatial derivatives. Implementations of these spatial filters will significantly increase the computational cost when compared with spatial derivatives involved in the divergence and curl operators (Yan and Sava, 2011).

EFFICIENT WAVE-MODE SEPARATION OPERATORS

In this section, we propose the efficient wave-mode separation operators in VTI media; basic formulations and computational details are included.

Formulations of separation operators

To project wavefields onto the qP-wave's exact polarization directions while keeping the implementation efficient, we take polari-

zation vectors as rotated wave vectors. One intuitional way to obtain the rotated wave vectors is to rotate the wave vector by $\Delta\theta$, defined as the deviation angle between the polarization vector and wave vector at each wavenumber; then, in 2D media, equation 1 can be rewritten as

$$q\tilde{P} = i\mathbf{k}' \cdot \tilde{\mathbf{U}} = ik_x'\tilde{U}_x + ik_z'\tilde{U}_z, \tag{2}$$

where $\mathbf{k}' = (k_x', k_z')$ is defined as a rotated wave vector to represent the qP-wave's polarization vector $\mathbf{P_{qP}}$ in equation 1. The explicit forms of rotated wave vectors can be obtained by considering local plane-wave propagations that fulfill the following relations (Berkhout, 1987):

$$(\sin\theta, \cos\theta) = (vk_x/\omega, vk_z/\omega), \tag{3}$$

where θ represents the phase angle of qP-wave with respect to the positive z-axis (consistent with the direction implied by wave vector) and ω is the angular frequency. Here, k_x and k_z are the x- and z-components of the original wave vector $\mathbf{k}$, respectively. Assuming that θ' is the angle of the qP-wave polarization's direction with respect to the positive z-axis, we have

$$\theta' = \theta + \Delta\theta. \tag{4}$$

Note that by defining θ' as in equation 4, the deviation angle $\Delta\theta$ can have either a positive or a negative value. After some algebraic calculation, we finally have the expression of the rotated wave vector as

$$\mathbf{k}' = \mathbf{R}\mathbf{k}, \tag{5}$$

where $\mathbf{R}$ is the rotation matrix with the following form:

$$\mathbf{R} = \begin{bmatrix} \cos\Delta\theta & \sin\Delta\theta \\ -\sin\Delta\theta & \cos\Delta\theta \end{bmatrix}, \tag{6}$$

the detailed derivations of equations 5 and 6 can be found in Appendix A.

To derive new separation operators, we substitute the rotated wave vector of equations 5 and 6 into equation 2, followed by an inverse Fourier transform on both sides of equation 2; finally, we have the proposed separation operator for extracting the qP-wave mode in space domain as

$$qP = D_x U_x + D_z U_z, \tag{7}$$

with

$$\begin{aligned} D_x &= \cos\Delta\theta\partial_x + \sin\Delta\theta\partial_z, \\ D_z &= \cos\Delta\theta\partial_z - \sin\Delta\theta\partial_x. \end{aligned} \tag{8}$$

Note that the deviation angle $\Delta\theta$ in equation 8 is now defined in the space domain and should be determined locally at each grid. Similarly, the separation operator for extracting the qS-wave mode in the 2D case can be easily derived out by using the orthogonality of polarization directions between the qP- and qS-waves as

$$qS = D_z U_x - D_x U_z. \tag{9}$$

It is easy to find that the proposed wave-mode separation operators 7 and 9 are linear combinations of spatial derivatives with rotations defined by deviation angle $\Delta\theta$. In isotropic media, deviation angle $\Delta\theta$ equals zero and operators 7 and 9 reduce to 2D divergence and curl operators. When compared with the divergence and curl separation operators for isotropic media, the main added computation cost of applying these operators in VTI media is to compute $\Delta\theta$, and neither Fourier transform nor spatial filtering is needed. Moreover, because the effect of anisotropy has been decomposed from the operations of projecting wavefields (Xu and Zhou, 2014), the deviation angles can be calculated locally in space. The present operators 7 and 9 can then be naturally adapted to heterogeneous media without any modifications. This is another advantage over applying conventional wave separation algorithms in heterogeneous media. In these algorithms, to achieve a compromise between accuracy and efficiency, several reference models are often chosen to approximate local heterogeneity. Then, wavefield projections have to be applied repeatedly using each reference model that further increases the computational cost (Yan and Sava, 2011; Cheng and Fomel, 2014).

Estimation of deviation angles

As we have illustrated above, the key factor to construct our separation operators 7 and 9 is the estimation of deviation angle $\Delta\theta$. To calculate $\Delta\theta$, we start from analytic expressions for polarization vectors in 2D VTI media (Rommel, 1994)

$$\begin{aligned} P_{\mathrm{qPx}} &= \sqrt{G_{33}/(G_{11}+G_{33})}, \\ P_{\mathrm{qPz}} &= \mathrm{sgn}(G_{13})\sqrt{G_{11}/(G_{11}+G_{33})}, \end{aligned} \tag{10}$$

where P_{qPx} and P_{qPz} are the x- and z-components of the qP-wave's polarization vectors, respectively. Here, G_{11}, G_{33}, and G_{13} are the Christoffel elements with the expressions

$$\begin{aligned} G_{11} &= \frac{1}{2}[(C_{11}-C_{44})n_x^2 - (C_{33}-C_{44})n_z^2] \\ &\quad -\frac{1}{2}\sqrt{[(C_{11}-C_{44})n_x^2-(C_{33}-C_{44})n_z^2]^2 + 4(C_{13}+C_{44})^2 n_x^2 n_z^2}, \\ G_{33} &= -\frac{1}{2}[(C_{11}-C_{44})n_x^2 - (C_{33}-C_{44})n_z^2] \\ &\quad -\frac{1}{2}\sqrt{[(C_{11}-C_{44})n_x^2-(C_{33}-C_{44})n_z^2]^2 + 4(C_{13}+C_{44})^2 n_x^2 n_z^2}, \\ G_{13} &= (C_{13}+C_{44})n_x n_z, \end{aligned} \tag{11}$$

where $\mathbf{n} = (n_x, n_z)$ is the unit wave vector that represents the local propagation direction. Here, C_{ij} is the stiffness coefficient.

Using the definitions of phase angle θ and polarization angle θ' as mentioned before, we can obtain the two angles as

$$\theta = \arctan(n_x/n_z) \tag{12}$$

and

$$\theta' = \arctan(P_{\mathrm{qPx}}/P_{\mathrm{qPz}}). \tag{13}$$

Then, the deviation angle $\Delta\theta$ can be calculated as

$$\Delta\theta = \arctan(P_{\mathrm{qPx}}/P_{\mathrm{qPz}}) - \arctan(n_x/n_z). \quad (14)$$

It is easy to see that once unit wave vectors $\mathbf{n} = (n_x, n_z)$ are obtained, it can be used to calculate polarization vectors through equations 10 and 11; then, θ and θ' are estimated using equations 12 and 13. Finally, $\Delta\theta$ can be obtained by equation 14.

Calculation of Poynting vectors

An efficient way to estimate the local propagation direction is using Poynting vectors (Yoon and Marfurt, 2006). The added computational cost for calculating the Poynting vector is minor because only derivatives in space and time are needed, which are easy to compute during two-way wave extrapolation. This method strongly depends on the assumption that there exists only one dominant direction of propagation at each grid during one-time step wave extrapolation. Although accounting for all propagation directions during wave propagation is possible through local plane-wave decomposition (Xie and Wu, 2002; Xu et al., 2011), this approach is very computational expensive for large-scale geophysical applications (Guan et al., 2013). Besides, as indicated often in geophysical literature, the propagation directions calculated by the Poynting vectors are reasonable approximations in many cases (Dickens and Winbow, 2011; Vyas et al., 2011; Yoon et al., 2011). As a result, we use the Poynting vectors to quickly estimate local propagation directions.

A straightforward way to calculate the Poynting vectors in elastic-wave extrapolation is using the Poynting vectors' definition in an elastic medium, i.e., the density of elastic energy flux defined as (Črenvý, 2001)

$$s_i = -\sigma_{ij} v_j, \quad (15)$$

where σ_{ij} and v_j are the stress tensor and particle velocity, respectively. The rule that repeated indices imply summation over these indices is used. However, in anisotropic media, the direction vectors calculated by equation 15 are consistent with group-velocity vectors, which are different from the directions of wave vector $\mathbf{n}$ (McGarry and Qin, 2013). Although the directions pointed by these two vectors can be transformed from each other through some analytical expressions (Tsvankin, 2005), it will add some computational complexity. We adopt another way to calculate Poynting vectors in the elastic case. First, the elastic wavefields are separated into qP- and qS-waves, and then we apply the acoustic Poynting vectors' definitions on the qP wavefield to obtain the local propagation directions (McGarry and Qin, 2013). This may cause some ambiguities: Because the purpose of the paper is to develop an efficient wave-mode separation method, how can we obtain the separated wavefields first? Well, this is because the separated wavefields here are only used to roughly estimate the propagation direction, they are not the final separated results, and the initial separated wavefields are not necessarily exact. Naturally, we can apply isotropic separation operators to obtain the initial qP wavefield in anisotropic media. After obtaining the initial qP wavefield, the Poynting vector $\mathbf{s}$ can be obtained according to its definition in the acoustic case (Yoon and Marfurt, 2006):

$$\mathbf{s} = -\dot{P}_0 \nabla P_0, \quad (16)$$

where ∇P_0 denotes the spatial gradient of the initial qP wavefield P_0 and $\dot{P}_0$ represents the time derivative of P_0. The unit wave vector $\mathbf{n} = (n_x, n_z)$ is then calculated as

$$n_x = s_x/|\mathbf{s}|, \quad n_z = s_z/|\mathbf{s}|. \quad (17)$$

Generate the initial quasi-P wavefield

As mentioned in the last section, we can apply a divergence operator onto any vector elastic wavefield to obtain the initial qP wavefield P_0. We take the velocity wavefield; for example, the initial qP wavefield can be expressed as

$$P_0 = \nabla \cdot \mathbf{V}, \quad (18)$$

where $\mathbf{V}$ is the particle velocity wavefield and $\nabla\cdot$ is the divergence operator. Substituting equation 18 into equation 16, we have

$$\mathbf{s} = \partial_t(\nabla \cdot \mathbf{V})\nabla(\nabla \cdot \mathbf{V}). \quad (19)$$

Because we use a set of first-order equations written in velocity-stress components for elastic-wave extrapolation in VTI media (Duveneck and Bakker, 2011), the spatial derivatives of $\nabla \cdot \mathbf{V}$ needed to form operator $\nabla(\nabla \cdot \mathbf{V})$ are not among the derivatives that are already computed in wavefield extrapolation. Because spatial derivatives' calculations account for most computing time in estimation of the Poynting vectors (assuming we use lower order accuracy for temporal derivative, which is true in practical computation), this means that a nonnegligible computational cost can be added if we define our initial qP wavefield in equation 18.

A more efficient way to obtain the initial qP wavefield P_0 is rewriting the divergence operation in forms of the stress tensor (Ha et al., 2014):

$$P_0 = \nabla \cdot \mathbf{U} = (\sigma_{xx} + \sigma_{zz})/(2\rho(V_{\mathrm{P}}^2 - V_{\mathrm{S}}^2)), \quad (20)$$

where $\mathbf{U}$ is the displacement wavefield, ρ is the density, and V_{P} and V_{S} are the P- and S-wave velocities, respectively. Equation 20 indicates that obtaining P_0 by applying divergence operator onto displacement wavefields can be represented by a simple weighted sum of the stress tensor. Again, we substitute equation 20 in equation 16, which yields alternative expressions for the Poynting vector:

$$\mathbf{s} = \partial_t(\sigma_{\mathrm{norsum}})\nabla(\sigma_{\mathrm{norsum}}), \quad (21)$$

with

$$\sigma_{\mathrm{norsum}} = (\sigma_{xx} + \sigma_{zz})/(2\rho(V_{\mathrm{P}}^2 - V_{\mathrm{S}}^2)). \quad (22)$$

Obviously, in this case, all the spatial derivatives needed for calculating Poynting vector $\mathbf{s}$ are only the first-order spatial derivatives of the stress tensor, which have been precomputed during numerically solving the velocity-stress coupled elastic-wave equation. Consequently, computational costs are reduced when using equation 21 instead of equation 19. In this paper, we adopt equation 21 to improve the efficiency of estimating the Poynting vectors.

Algorithm for efficient wave-mode separation in VTI media

The following steps summarize the whole procedure of wave-mode separation using the proposed efficient separation operators:

1) Use full anisotropic elastic-wave equation extrapolation, the specific forms of equations in VTI media are derived by Duveneck and Bakker (2011).
2) Calculate initial qP wavefield P_0 using the isotropic separation operator 20.
3) Calculate Poynting vector **s** using equation 21 and unit wave vector **n** using equation 17.
4) Estimate deviation angle $\Delta\theta$ using its relations with unit wave vector **n** through equations 10–14.
5) Apply the proposed separation operators 7 and 9 to obtain the final separated qP- and qS-waves in 2D VTI media.

PHASE AND AMPLITUDE CORRECTIONS

Wave-mode separation is one of the key steps in elastic-wave migration (Yan and Sava, 2008). However, phase and amplitude of the waveforms are changed by applying separation operators in wave-mode separation. To obtain seismic images with correct physical meanings, the waveforms changes must be corrected (Sun et al., 2011). In isotropic wave-mode separation, waveform changes by applying the divergence and curl operators are comprehensively investigated by Sun et al. (2001, 2011) through substituting a plane-wave trial solution into the divergence and curl operators. Duan and Sava (2015) analyze the waveforms changes by rewriting the spatial derivatives using the dispersion relationship in the wavenumber domain. They also propose correction methods for such waveform changes. Due to the similarity between our operators and the isotropic separation operators, we can easily adopt the correction methods developed in the isotropic case into the proposed operators. Note that the direction cosines of deviation directions $(\cos\Delta\theta, \sin\Delta\theta)$ are normalized vectors and they will not affect physical quantities; then, only corrections for waveform changes resulting from the spatial derivatives in operators 7 and 9 are needed for using the divergence and curl operators. We start illustrating corrections for our operators with the method proposed by Duan and Sava (2015); then, we reformulate their approach and give a different implementation to investigate the physical meanings implied in the correction methods. The spatial derivative in the wavenumber domain can be expressed as (Duan and Sava, 2015)

$$i\mathbf{k} = i\frac{\omega}{v}\mathbf{n}, \tag{23}$$

where v is the phase velocity corresponding to different wave modes. Using equation 23, the correction operator **G**, which equals $1/i\mathbf{k}$, can be written as

$$\mathbf{G} = \frac{v}{i\omega}\mathbf{n}, \tag{24}$$

by introducing the sign function sgn, and after some calculations, the correction operators can be finally given by

$$\mathbf{G} = \frac{-iv\,\mathrm{sgn}(\omega)}{|\omega|}\mathbf{n}. \tag{25}$$

The phase correction term in equation 25 is $-i\,\mathrm{sgn}(\omega)$, which is a Hilbert transform that causes a $\pi/2$ phase shift. To improve the computational efficiency of calculating the Hilbert transform of the wavefields, we follow Hu et al.'s. (2015) approach by implementing the Hilbert transform to the source wavelet before wavefield extrapolations. To apply amplitude correction, an additional filter $1/|\omega|$ should be applied on the source wavelet, followed by multiplying rescale factor v with the extrapolated wavefields.

Because the correction operator 25 is the reciprocal of the spatial derivative (equation 23), the physical units of separated wave modes after applying equation 25 are also corrected back to the same as that of input vector wavefields. As a result, we can directly compare the separated wave modes with input elastic wavefields. After corrections, the following equation is fulfilled:

$$|\mathrm{qP}_{\mathrm{scalar}}| = |\mathbf{qP}|, \tag{26}$$

where $|\mathrm{qP}_{\mathrm{scalar}}|$ is the absolute value of the corrected scalar qP wave's amplitude extracted by equation 7 and $|\mathbf{qP}|$ represents the qP-wave's norm in the input vector wavefields. A similar equation can be derived out for the qS-wave in the 2D case. In the 3D case, because the curl is a vector, equation 26 should be modified by replacing the left side of equation 26 with the norm of the corrected qS-wave vectors. Equation 26 implies that wave energy is conserved in wave-mode separation. The fulfillment of equation 26 is important in elastic-wave migration based on the scalar imaging condition (Sun et al., 2011). The scalar imaging condition seeks to obtain unique PS and SP images that reflect the energy conversion strength between different wave modes at an interface (Duan and Sava, 2015). As a result, the energy conservation property indicated by equation 26 is a prerequisite to obtain seismic images with the right energy relationships. Note that by implementing correction operators 25, most parts of calculations are applied on the source wavelet before wavefield extrapolations; the only part left is multiplying the rescale factor v with extrapolated wavefields, which can barely affect the computational efficiency.

NUMERICAL TEST

This section contains three numerical examples. They are for a homogeneous VTI model, a two-layer VTI model, and a partial Sigsbee model.

Homogeneous VTI model

First, we verify the effectiveness of our separation operators on a homogeneous VTI model with vertical velocity $V_{\mathrm{P}}^0 = 3$ km/s and $V_{\mathrm{S}}^0 = 1.73$ km/s and anisotropic parameters $\epsilon = 0.25$ and $\delta = -0.29$. The model ranges from 0 to 4000 m and grid interval is 10 m in the x- and z-directions. The stiffness coefficients in equation 11 have been converted to Thomsen's (1986) parameters for consistency of computation. Wavefields are generated based on the full-anisotropic elastic-wave equation, as has been mentioned in the algorithm section. The finite-difference method on a staggered grid (Virieux, 1986) with 10th-order accuracy in space and second-order accuracy in time is used for numerically solving the equations and the perfectly matched layer/absorbing boundary condition (Bérenger, 1994) is applied to all grid edges.

Figure 1a and 1b demonstrates snapshots for x- and z-components of velocity wavefields at 500 ms. It is clear that the qP- and qS-waves are coupled with each other. The initial qP wavefield is shown in Figure 1c. We also present the corresponding initial qSV wavefield (using curl operators) in Figure 1d for comparison, although the initial qSV component will not be used in the follow-

ing estimation of the deviation angles. As expected, the separation is incomplete in the initial qP- and qS-waves because the elastic wavefields are not projected onto the correct polarization directions for each wave mode by isotropic separation operators. However, when compared with the original elastic wavefields, the coupled energy of the SV-wave is reduced in the initial qP wavefield. As has been mentioned before, the purpose of obtaining the initial qP wavefield is to further estimate the wave-propagation directions; a qP wavefield with a small part of the qS-wave can fulfill our requirement.

Figure 2a shows the estimated deviation angles. As we can see, the deviation angles are zero along the symmetry axis and within the symmetry plane, which is consistent with the difference between polarization vectors and wave vectors (Tsvankin, 2005). It is also very clear that the deviation angles for a qP-wave are coupled with qS-wave energy because we use incomplete separated qP wavefields for calculation. We should mention that these unwanted qS-wave artifacts in the estimated deviation angles can barely affect the effectiveness of the proposed separation operators 7 and 9. This is because the most useful information, i.e., the deviation angle $\Delta\theta$ between the wave vectors and polarization vectors for the qP-wave has been successfully obtained, and the separation results are almost always much better than the isotropic separation operators. However, if the unwanted qS-wave artifacts contaminate the useful deviation angle $\Delta\theta$ of the qP-wave, then the projection directions implied by equations 7 and 9 will not be accurate anymore. As a result, crosstalk artifacts will be generated. We will discuss this issue later in our second numerical example.

Figure 1e and 1f demonstrates the separated wavefields using the proposed separation operators without applying the correction operator 25. Compared with the separation results using isotropic separation operators as illustrated in Figure 1c and 1d, crosstalk artifacts are greatly suppressed because wave modes have been projected onto the right directions in which they are orthogonally polarized. To correct for amplitude and phase changes introduced by spatial derivatives involved in separation operators 7 and 9, we then apply correction operator 25 in wave-mode separation; the results are shown in Figure 2b and 2c. Apparently, the phases of the waveforms between the corrected and uncorrected wave modes are different. To have a detailed insight into the effects of the correction operators, one selected trace at distance 1700 m with different correction terms is compared. We take the trace with the amplitude and phase corrections as the reference trace. Figure 3a shows a comparison between the reference trace and the trace with amplitude correction only. Obviously, the amplitude-corrected trace differs from the reference trace with $\pi/2$ phase shift while keeping the amplitude at the same level. Figure 3b displays a comparison between the reference trace and the trace with phase correction only. In this case, the phase-corrected trace is consistent with the reference trace on the phase although with a distinctly lower amplitude level.

To prove that the corrected wavefields are more reasonable for elastic-wave imaging, the energy relationship conservation equation 26 is verified. Figure 4 shows comparisons between the absolute value of the corrected wavefields' amplitude (left side of equation 26) and the norms of the input velocity wavefields (right

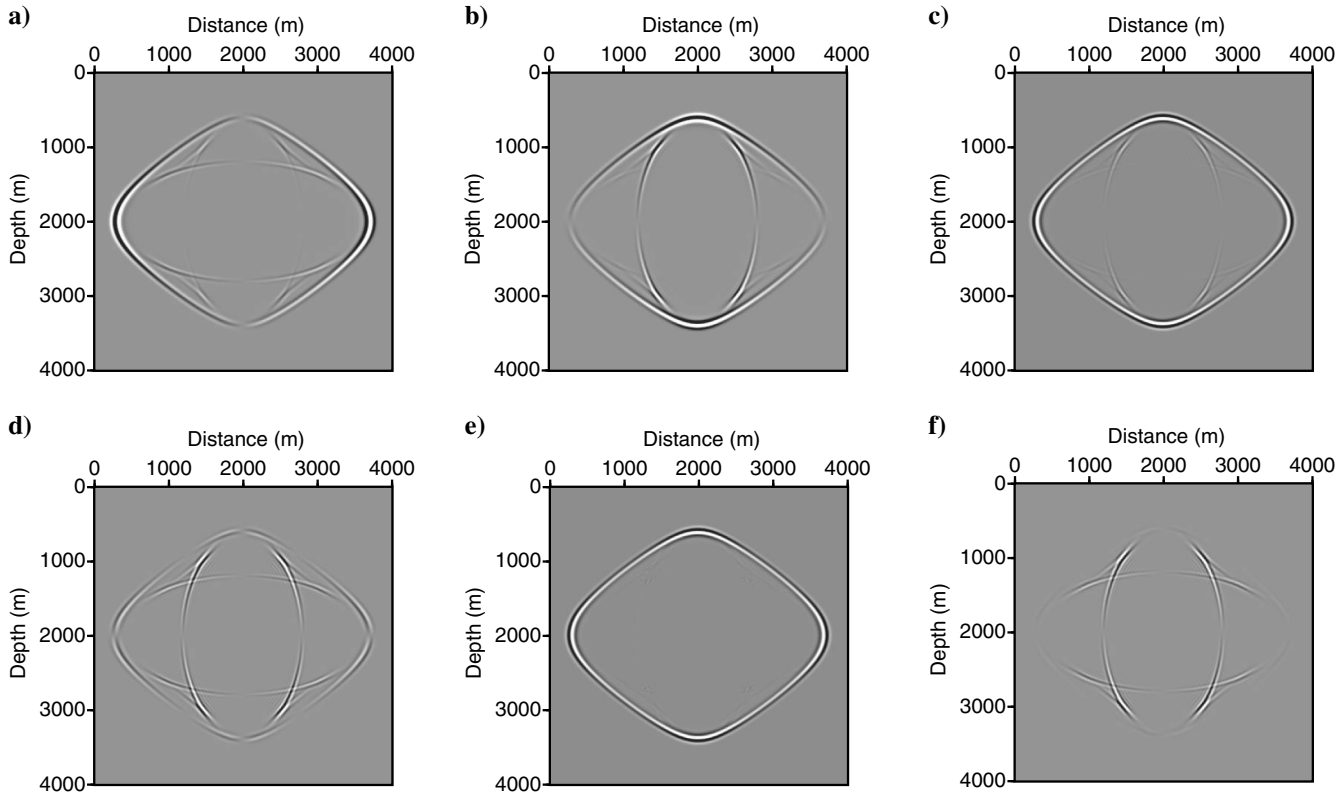

Figure 1. (a and b) Input x- and z-components of velocity wavefields for a homogeneous VTI model with $\varepsilon = 0.25$ and $\delta = -0.29$. (c and d) Separated qP- and qS-waves using the divergence and curl operators (initial separated wavefields for calculating the Poynting vectors). (e and f) Separated qP- and qS-waves using the separation operators proposed in this paper; correction operator 25 is not applied.

side of equation 26). Figure 4a and 4c shows comparisons for the separated qP wavefield (due to the symmetry, only a half range in the x-direction is displayed) and a magnified display of five selected traces. Figure 4b and 4d demonstrates results for the qS wavefield. Clearly, the two values match very well with each other. In Figure 4a and 4c, curves that represent the separated qP-wave's absolute amplitude (dashed red line) are completely fitted with norm curves that belong to the qP-wave's energy in input wavefields (solid blue line), whereas all the norm curves stand for the qS-wave's energy in input wavefields that are left untouched. Similar results are obtained for the separated qS-wave as displayed in Figure 4b and 4d. The results indicate that the energy relationships among different wave modes remain unchanged in wave-mode separation by using corrections. As we have mentioned before, the scalar-imaging condition in elastic migration aims to represent the energy conversion strength of different wave modes in the subsurface; then, applying correction operation 25 becomes necessary in anisotropic elastic-wave migration.

Two-layer model

On our second numerical example, we use a two-layer VTI model for illustration. The model ranges from 0 to 4000 m, and the grid interval is 10 m in the x- and z-directions; the reflection layer is inserted at a depth of 1500 m. The velocity V_P^0 ranges from 3 to 4 km/s, and V_S^0 ranges from 1.73 to 2.3 km/s; anisotropy parameter ε ranges from 0.2 to 0.24, and δ ranges from 0.1 to 0.15. The same finite-difference scheme is used as in our first example. Figure 5a and 5b shows snapshots for x- and z-components of velocity wavefields at 900 ms. The extracted qP- and qS-waves using the divergence and curl operators are shown in Figure 5c and 5d. Clearly, there exist residuals corresponding to the qS-wave in the extracted qP-wave and qP-wave residuals in the extracted qS-wave. Figure 5e and 5f demonstrates results using the separation operators proposed in this paper. Obviously, much better separation results are obtained for both separated waves; the qS-wave's energy is significantly removed from the separated qP-wave, and vice versa.

It is also visible that some minor qS-wave residuals exist in particular areas of the separated qP-wave. The qS-wave residuals exist because the projection directions implied by operators 7 and 9 in these areas are wrong when compared with the exact polarization directions. This can be verified from the estimated deviation angles as displayed in Figure 6a. It is easy to notice the area where there exist overlapping events (the area indicated by the black window in Figure 6a), which disproves the assumption of one propagation direction implied in the Poynting vector calculations. As a result, the accuracy of the estimated deviation angles is degraded and crosstalk artifacts appear. Luckily, as we have mentioned before, the proposed separation operators are constructed with isotropic separation operators by additional rotation. This means that even if we can only obtain part of the accurate deviation angles in a very complex model

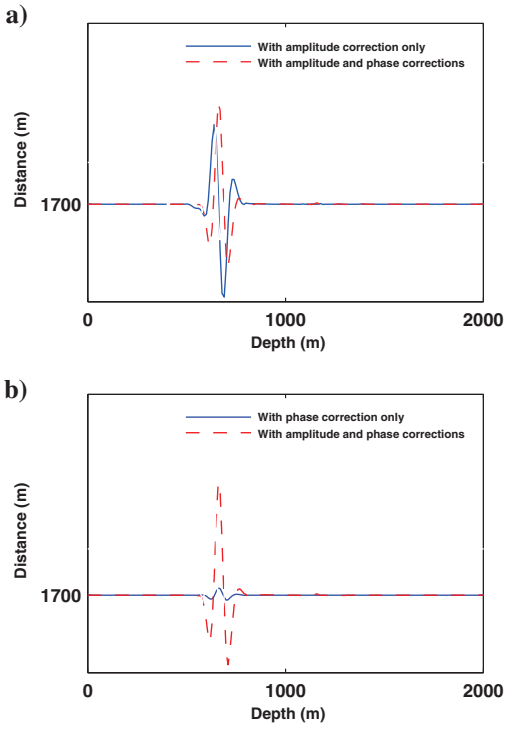

Figure 3. Comparisons for the homogeneous VTI model between the trace with corrections (amplitude and phase, solid blue line) and the trace (a) with amplitude correction only (dashed red line), and (b) with phase correction only (dashed red line).

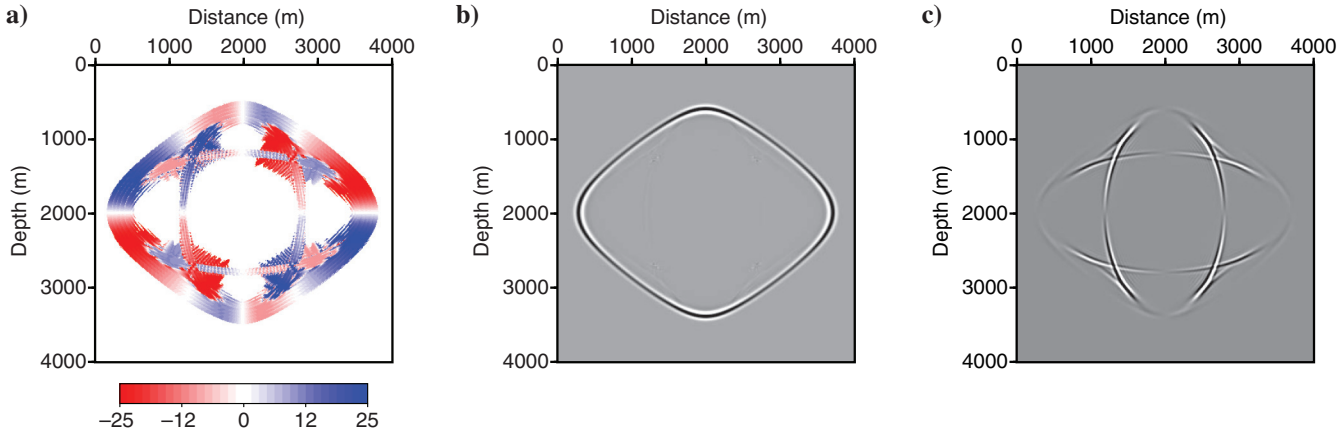

Figure 2. (a) Estimated deviation angles (°) between the wave vectors and polarization vectors for homogeneous VTI model. (b and c) Separated qP- and qS-waves using the separation operators proposed in this paper; correction operator 25 is applied.

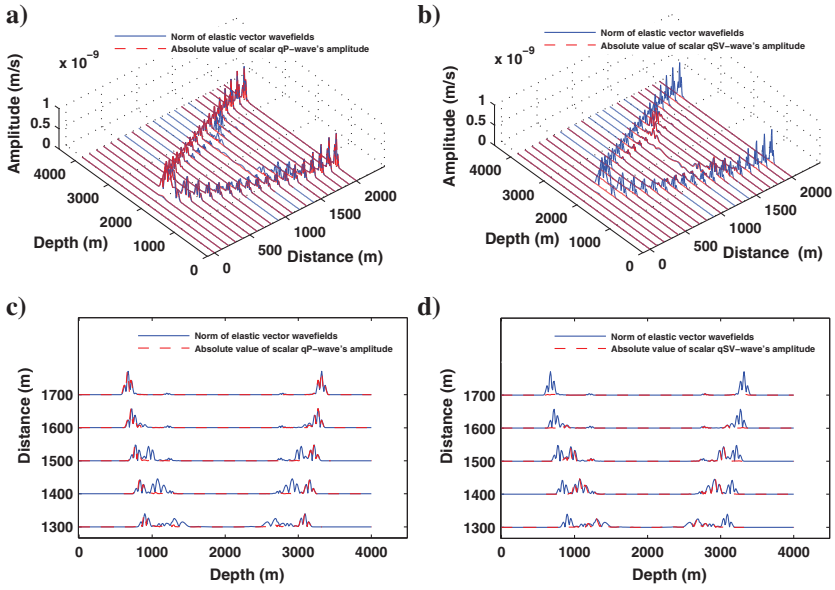

Figure 4. Comparisons for the homogeneous VTI model between the norms of input velocity wavefields (solid blue lines) with absolute value of the corrected wavefields' amplitude (dashed red lines). (a) Comparisons for the separated qP-wave. (c) Magnified display of five selected traces in (a) (note that the outer solid lines in blue refer to the qP-wave components in the original velocity wavefields due to the faster phase velocity). (b) Comparisons for the separated qS-wave. (d) Magnified display of five selected traces in (b) (note that the inner solid lines in blue refer to the qS-wave components in the original velocity wavefields due to the slower phase velocity).

by using the Poynting vectors, the separation results generated by the proposed separation operators will always be improved when compared with the divergence and curl operators, which makes our operators robust to implement.

The wavefields separated by applying correction operator 25 are illustrated in Figure 6b and 6c. The waveform phases are clearly corrected when compared with those without corrections. Figure 7 shows comparisons between the absolute value of the corrected wavefields' amplitude and the norms of the input velocity wavefields. Again, it is easy to see that the energy relationships of different wave modes remain unchanged in wave-mode separation with corrections.

Sigsbee model

To test our operators' abilities to adapt to complex geologic structures in wave-mode separation, part of the Sigsbee model is used for a test. The model is modified from the Sigsbee model (Paffenholz et al., 2002), and the model parameters are shown in Figure 8. Figure 9a and 9d demonstrates snapshots for the x- and z-components of the velocity wavefields at 1250 ms. We can see that the wavefields are

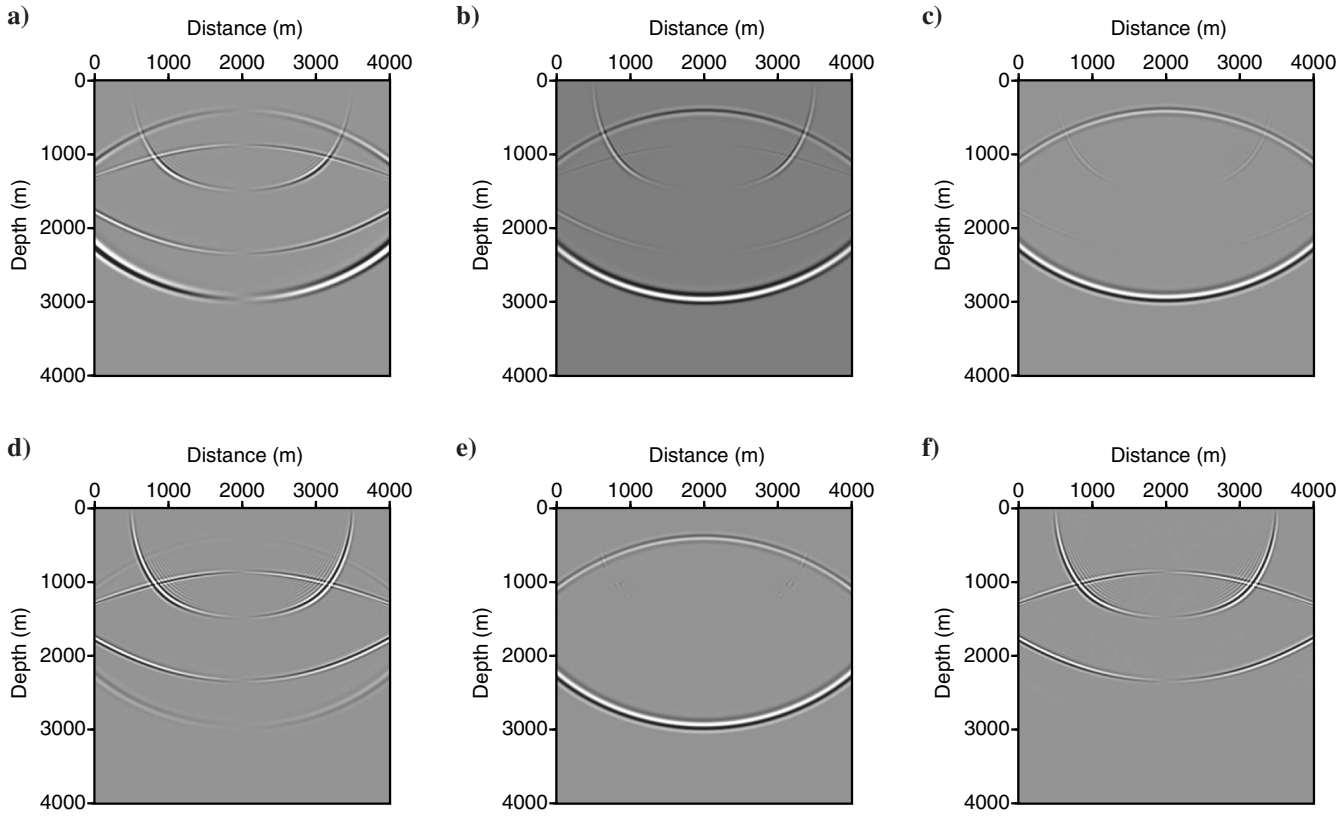

Figure 5. (a and b) Input x- and z-components of velocity wavefields for a two-layer VTI model; the parameters used are as described in our second numerical example. (c and d) Separated qP- and qS-waves using the divergence and curl operators. (e and f) Separated qP- and qS-waves using the separation operators proposed in this paper; correction operator 25 is not applied.

complex and that multiple propagation paths exist in many areas. The complexity of the wavefields can also be verified on the estimated deviation angles, as shown in Figure 10. As we can see, the deviation angles are noisy and many overlapping events appear due to wave propagation in different directions at a single grid. Naturally, one may expect that the separated wavefields are dirty and unstable, which is consistent with the qualities of the estimated deviation angles.

However, we again obtain better results using proposed separation operators, as shown in Figure 9. The qS-wave residuals at the distances $x = 13{,}000$ and 17,000 m with depth of $z = 7000$ m are obvious in the separated qP-wave using the divergence operator as displayed in Figure 9b. Similarly, there exist qP-wave residuals in the separated qS-wave at $x = 11{,}000$ m and $z = 7000$ m using the curl operator, as demonstrated in Figure 9c. As a comparison, the crosstalk artifacts mentioned above are attenuated when the proposed separation operators are applied as shown in Figure 9e and 9f.

Comparisons between the separated wavefields by applying the correction operator 25 and the input elastic wavefields are shown in Figure 11. As we can see, although the wavefields are complex in this case, the good fitness of the energy peaks for different wave modes is clearly demonstrated. Our numerical example on the Sigsbee model indicates that the proposed separation operators are a robust implementation even in a complex model.

DISCUSSION

Extension to 3D VTI media

This paper is mainly focused on the concept of newly proposed separation operators. So far, we have only verified the proposed operators in 2D VTI media. In 3D VTI media, due to the qP-wave's faster phase velocity for all propagation directions when compared with the qS-wave modes, implementation of the projection for separating the qP-wave has the same form as its counterpart in the 2D case (Dellinger, 1991). This means that the qP-wave's separation operator 7 can be directly extended to the 3D case. However, a qSV-wave polarized in the symmetry-axis plane and a qSH-wave polarized in the isotropy plane are allowed in 3D VTI media, and decoupling these two kinds of qS-wave modes is challenging. This is because of the qS-wave singularities, which means there exist directions where the qSV- and qSH-waves have the same phase velocity. As a result, the polarization vectors are not uniquely defined for each qS-wave mode, and additional information is needed to define the qSV- and qSH-wave polarization

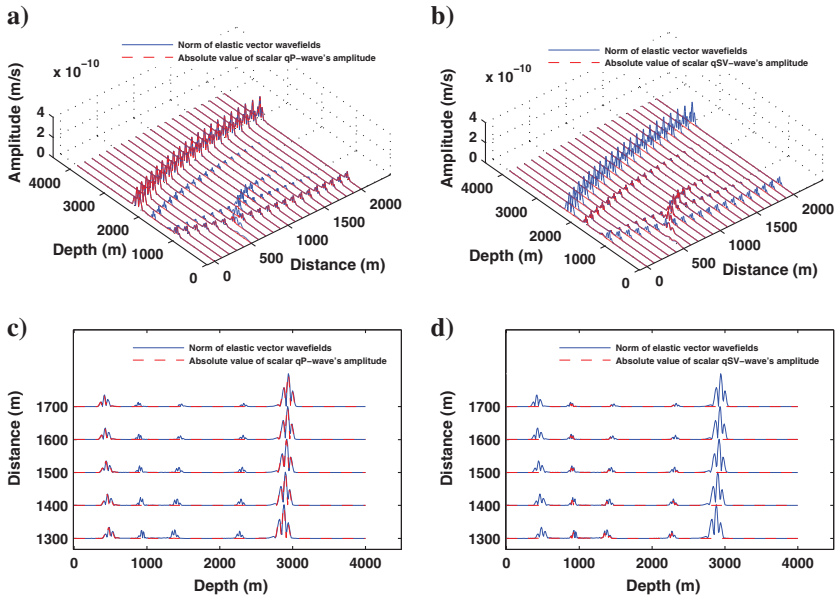

Figure 7. Comparisons for the two-layer VTI model between the norms of the input velocity wavefields (solid blue lines) with the absolute value of the corrected wavefields' amplitude (dashed red line). (a) Comparisons for the separated qP-wave. (c) Magnified display of the five selected traces in (a). (b) Comparisons for the separated qS-wave. (d) Magnified display of the five selected traces in (b).

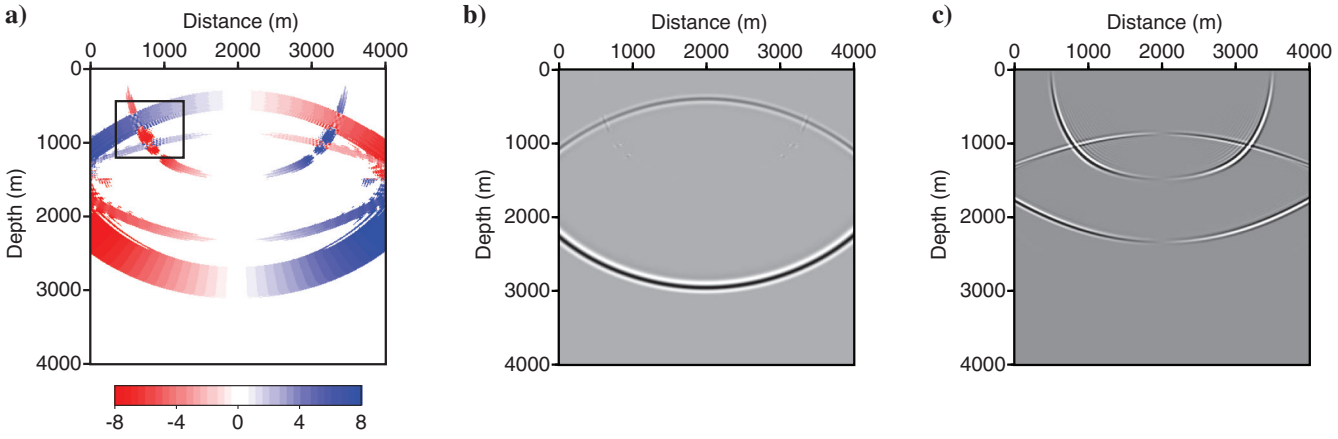

Figure 6. (a) Estimated deviation angles (°) between the wave vectors and polarization vectors for a two-layer VTI model. (b and c) Separated qP- and qS-wave modes using the separation operators proposed in this paper; correction operator 25 is applied. Note the overlapping events due to multiple propagation paths as indicated in (a) with the black window.

vectors. Yan and Sava (2009a) propose using the mutual orthogonality among the three wave modes to remove singularities and verify their method's effectiveness using synthetic data set. Luckily, in their approach, the determination of the qP-wave's polarization vectors is still one of the key steps, so we can adopt the similar singularity-removing approach, with an efficient way to calculate the polarization vectors as proposed in this paper. The extension of the present work to 3D VTI case is one of our future works.

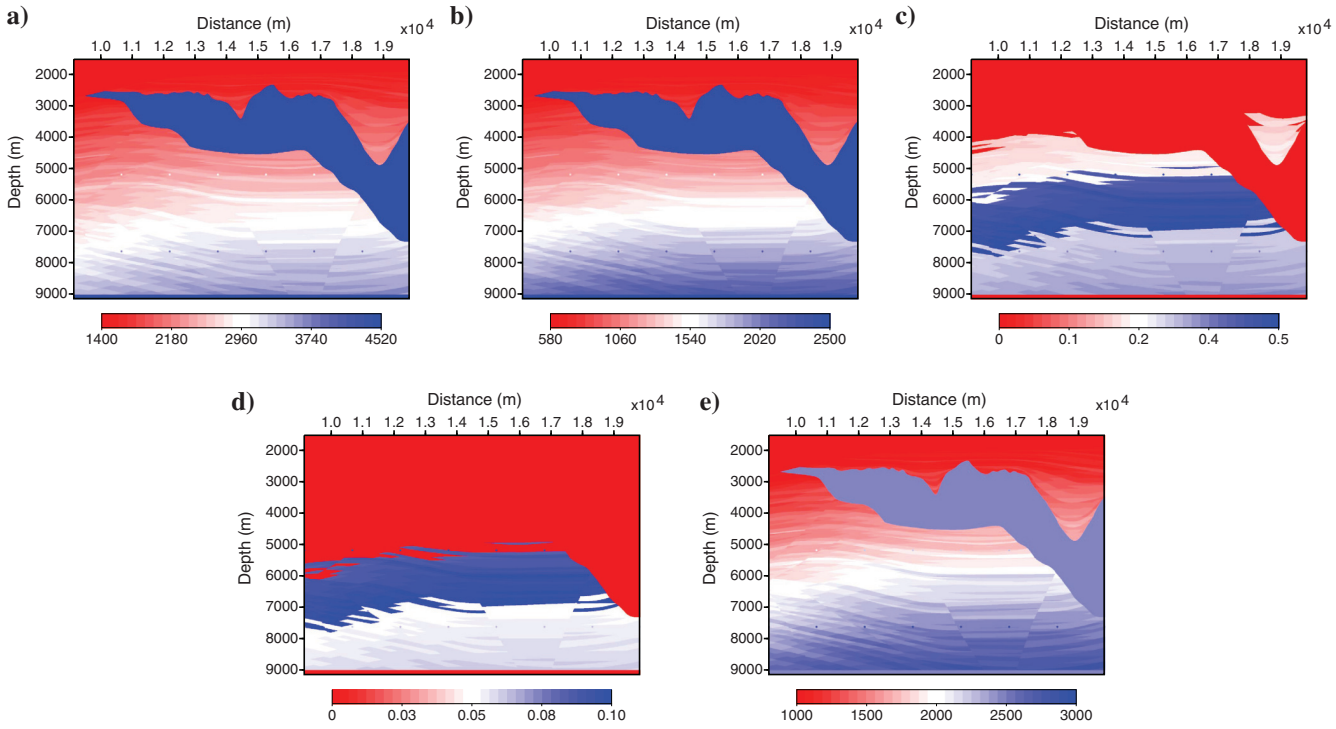

Figure 8. Partial Sigsbee model. (a and b) Partial V_P and V_S model; the physical units are meters per second. (c and d) Partical epsilon and delta model. (e) Partial density model; the physical unit is kilograms per cubic meter.

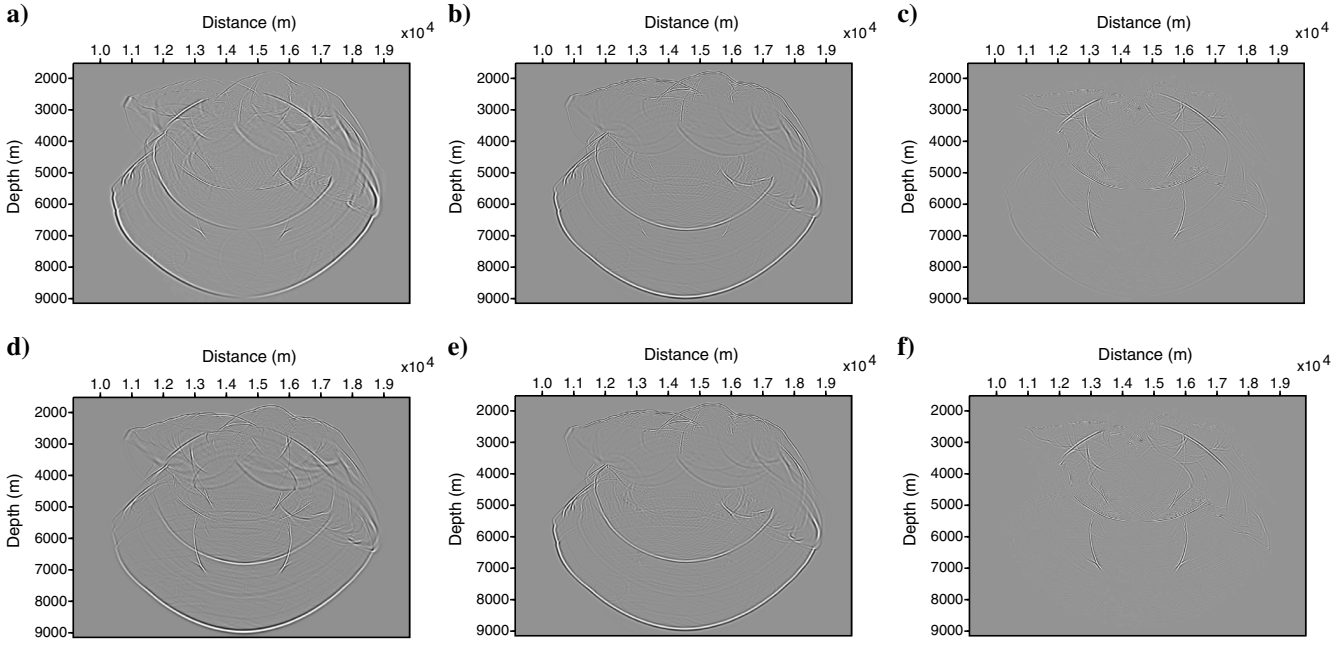

Figure 9. (a and d) Input x- and z-components of velocity wavefields for partial Sigsbee model as displayed in Figure 8. (b and c) Separated qP- and qS-waves using the divergence and curl operators. (e and f) Separated qP- and qS-waves using the separation operators proposed in this paper.

Relation to conventional wavenumber-domain-based methods

Here, we give more detailed illustrations about relations between the proposed method and the conventional wavenumber-domain-based methods. The two methods adopt the same physics as the orthogonality of polarization directions between P- and SV-waves in their polarized plane. Both methods attempt to project wavefields onto mutually orthogonal polarization directions for wave-mode separation. Taking the extracting qP-wave component as an example, both methods are based on the projection relation demonstrated by equation 1. The differences between these two methods lie in the specific implementations of the wavefield projection. The conventional wavenumber-domain methods directly use polarization vectors as project operators. As we have discussed in previous sections, implementing wave-mode separation under such a framework, either in the wavenumber domain by Fourier transforms (Dellinger and Etgen, 1990; Zhang and McMechan, 2010) or in the space domain by spatial filters (Yan and Sava, 2009b), is computationally expensive, especially for a large-scale model with high heterogeneity (Yan and Sava, 2011; Cheng and Fomel, 2014).

As a comparison, inspired by the deviation angles between the polarization vectors and the wave vectors in the wavenumber domain as shown in Figure 12a and 12c, the proposed method attempts to use wave vectors plus rotation to represent polarization vectors as illustrated in equation 5. Figure 12b and 12d shows the directions of the qP-wave's polarization vectors and rotated wave vectors. As we can see, the directions implied by these two vectors are consistent with each other. This is a verification that the proposed method equivalently implements wavefield projection following equation 1 as conventional wavenumber domain-based methods. However, by representing polarization vectors as rotated wave vectors using relation 5 instead of directly using their original definitions as in equation 10, the new expressions can benefit from the simplicities of the isotropic separation operators associated with the wave vectors. The space-domain representations of newly expressed polarization vectors become linear functions of the divergence and curl operators expressed as equations 7 and 9, which are easy to compute. The coefficients in front of the divergence and curl operators are determined by the deviation angles defined as in equation 14. The spatial deviation angles depend on the local propagation directions and represent the differences between polarization and wave vectors' directions at different phase angles, which correspond to deviation angles defined at different wavenumbers in the wavenumber domain. As a result, projections (equation 1) are now implemented in a more efficient way through the proposed method than by conventional wavenumber-domain separation methods.

As for numerical accuracy, the conventional wavenumber-domain-based methods are accurate for homogeneous media. In heterogeneous media, to improve the computational efficiency, accuracy is sacrificed by approximating local heterogeneity with several homogeneous reference models. The approximations not only cause separation errors but also increase the computational cost because wavefield projections have to be applied repeatedly using each reference model (Yan and Sava, 2011). On the contrary, the implementations of the proposed method remain exactly the same in the homogeneous and heterogeneous cases. This is because the deviation angles (equation 14) are locally calculated. The numerical errors of the proposed method come from the assumption of applying the Poynting vectors, as we have discussed in the "Numerical test" section The assumption breaks the perfection but not the effectiveness of the proposed method even in complex geology, as we have seen in numerical examples. Because the proposed method can always pro-

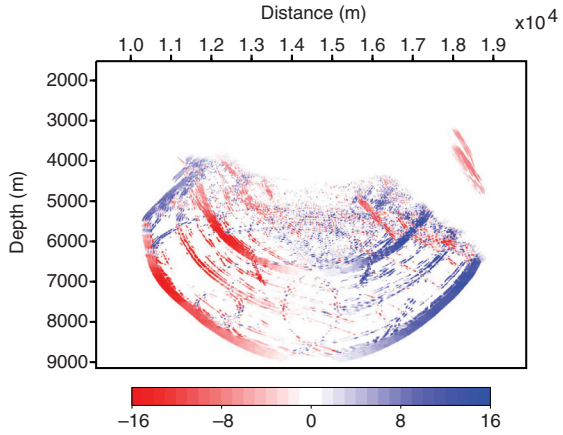

Figure 10. Estimated deviation angles (°) between the wave vectors and polarization vectors for the partial Sigsbee model.

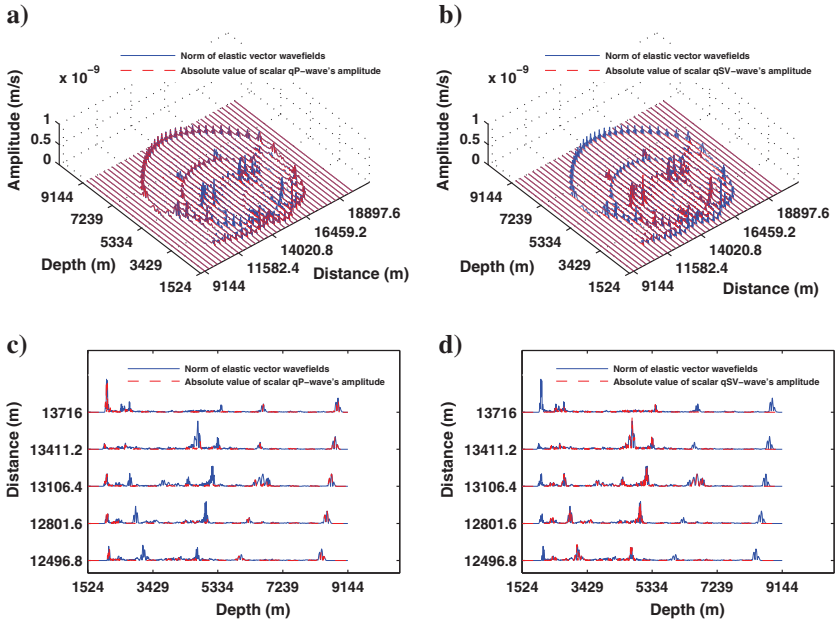

Figure 11. Comparisons for the partial Sigsbee model between the norms of the input velocity wavefields (solid blue lines) with the absolute value of the corrected wavefields' amplitude (dashed red line). (a) Comparisons for the separated qP-wave. (c) Magnified display of five selected traces in (a). (b) Comparisons for the separated qS-wave. (d) Magnified display of five selected traces in (b).

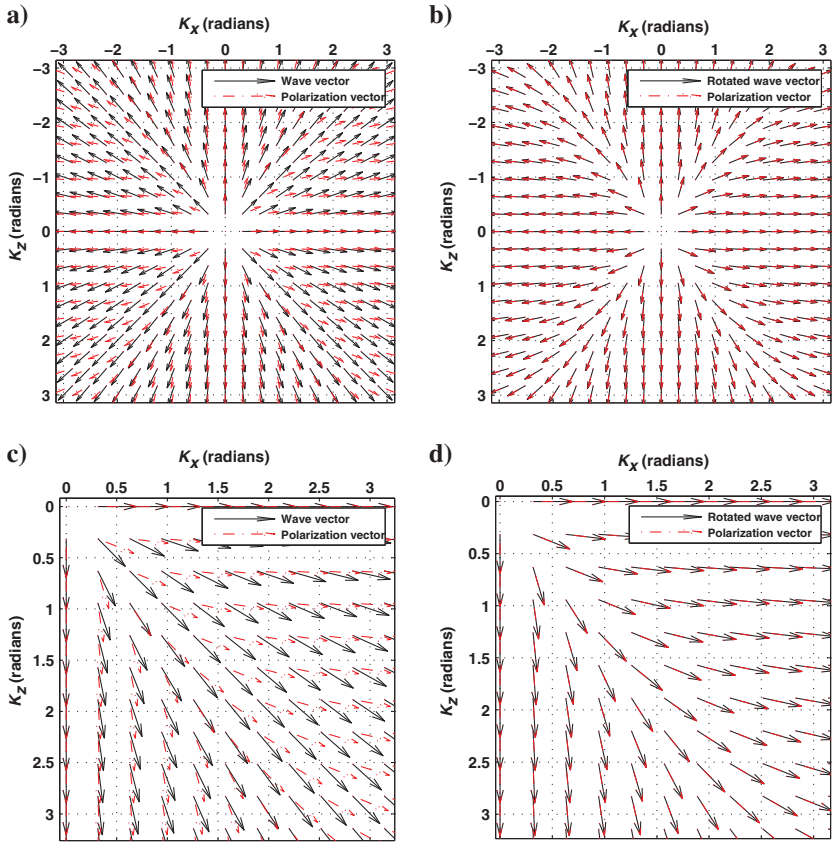

Figure 12 Directions of the qP-wave's wave vectors, rotated wave vectors, and polarization vectors as functions of the wavenumbers for a homogeneous VTI model with $\varepsilon = 0.25$ and $\delta = -0.29$. (a) Directions of the polarization vectors (dashed red dot arrows) and wave vectors (solid black arrows). (c) Magnified display from 0 radians to $+\pi$ radians of (a). (b) Directions of the polarization vectors (dashed red dot arrows) and the rotated wave vectors (solid black arrows). (d) Magnified display from 0 radians to $+\pi$ radians of (b).

vide improved separation results when compared with the divergence and curl operators with a minor added computational method, we believe that the development of the proposed method is still valuable.

CONCLUSION

In this paper, we have proposed new operators for efficient wave-mode separation in 2D VTI media. These operators are determined by locally rotating wave vectors to directions where the qP-wave is polarized, together with the orthogonality of the polarization directions between the qP- and qS-waves. When transformed into the space domain, the proposed operators become linear combinations of rotated spatial derivatives. These features of the new operators make wave-mode separation very efficient to implement. To correct for waveform changes caused by applying separation operators, phase and amplitude corrections are also introduced in this paper. The corrections can be applied with a small computational cost. Numerical examples demonstrate that the proposed operators provide separated wave modes with many fewer unwanted crosstalk artifacts when compared with the divergence and curl operators. Meanwhile, the wavefield energy is conserved by using the corrections in wave-mode separation.

ACKNOWLEDGMENTS

We acknowledge the support from the sponsors of WPI at Tongji University. We thank J. Etgen, I. Ravve, A. Stovas, and two anonymous reviewers for their valuable comments and suggestions.

APPENDIX A

DERIVATION OF THE ROTATED WAVE VECTOR

This appendix gives the derivation of rotated wave vector $\mathbf{k}'$ given in the main text. We start from equation 3, which describes the local plane-wave propagation, then the rotated wave vector $\mathbf{k}' = (k_x', k_z')$ also following the local plane-wave propagation relation,

$$(\sin\theta', \cos\theta') = (vk_x'/\omega, vk_z'/\omega), \quad \text{(A-1)}$$

using trigonometric relations,

$$\sin(\theta + \Delta\theta) = \sin\theta\cos\Delta\theta + \cos\theta\sin\Delta\theta \quad \text{(A-2)}$$

and

$$\cos(\theta + \Delta\theta) = \cos\theta\cos\Delta\theta - \sin\theta\sin\Delta\theta, \quad \text{(A-3)}$$

where together with equations 3 and 4, we have

$$k_x' = k_x\cos\Delta\theta + k_z\sin\Delta\theta \quad \text{(A-4)}$$

and

$$k_z' = -k_x\sin\Delta\theta + k_z\cos\Delta\theta. \quad \text{(A-5)}$$

Equations A-4 and A-5 are consistent with their matrix forms, as shown by equations 5 and 6.

REFERENCES

Bérenger, J. P., 1994, A perfectly matched layer for the absorption of electromagnetic waves: Journal of Computational Physics, **114**, 185–200, doi: 10.1006/jcph.1994.1159.

Berkhout, A. J., 1987, Applied seismic wave theory: Elsevier.

Červený, V., 2001, Seismic ray theory: Cambridge University Press.

Cheng, J., and S. Fomel, 2014, Fast algorithms for elastic-wave-mode separation and vector decomposition using low-rank approximation for anisotropic media: Geophysics, **79**, no. 4, C97–C110, doi: 10.1190/geo2014-0032.1.

Dellinger, J., 1991, Anisotropic seismic wave propagation: Ph.D. thesis, Stanford University.

Dellinger, J., and J. Etgen, 1990, Wavefield separation in two-dimensional anisotropic media: Geophysics, **55**, 914–919, doi: 10.1190/1.1442906.

Dickens, T. A., and G. A. Winbow, 2011, RTM angle gathers using Poynting vectors: 81st Annual International Meeting, SEG, Expanded Abstracts, 3109–3113.

Duan, Y., and P. Sava, 2015, Scalar imaging condition for elastic reverse time migration: Geophysics, **80**, no. 4, S127–S136, doi: 10.1190/geo2014-0453.1.

Duveneck, E., and P. M. Bakker, 2011, Stable P-wave modeling for reverse time migration in tilted TI media: Geophysics, **76**, no. 2, S65–S75, doi: 10.1190/1.3533964.

Guan, H., P. Williamson, B. Denel, F. Audebert, and B. Duquet, 2013, Angle-domain common-image gathers extracted from pre-stack RTM images: 83rd Annual International Meeting, SEG, Expanded Abstracts, 3767–3772.
Ha, J., S. Shin, W. Chung, and C. Shin, 2014, Efficient elastic reverse-time migration for decomposed P-wavefield using stress tensor in time domain: 84th Annual International Meeting, SEG, Expanded Abstracts, 4049–4054.
Hu, J. T., H. Z. Wang, and X. W. Wang, 2015, Angle gathers from reverse time migration using analytic wavefield propagation and decomposition in the time domain: Geophysics, **81**, no. 1, S1–S9, doi: 10.1190/geo2015-0050.1.
McGarry, R., and Y. Qin, 2013, Direction-vector-based angle gathers from anisotropic elastic RTM: 83rd Annual International Meeting, SEG, Expanded Abstracts, 3820–3824.
Paffenholz, J., B. McLain, J. Zaske, and P. Keliher, 2002, Subsalt multiple attenuation and imaging: Observations from the Sigsbee2B synthetic data set: 72nd Annual International Meeting, SEG, Expanded Abstracts, 2122–2125.
Rommel, B. E., 1994, Approximate polarization of plane waves in a medium having weak transverse isotropy: Geophysics, **59**, 1605–1612, doi: 10.1190/1.1443549.
Sun, R., J. Chow, and K.-J. Chen, 2001, Phase correction in separating P- and S-waves in elastic data: Geophysics, **66**, 1515–1518, doi: 10.1190/1.1487097.
Sun, R., G. A. McMechan, and C.-H. Chen, 2011, Amplitude balancing in separating P- and S-wave in 2D and 3D elastic seismic data: Geophysics, **76**, no. 3, S103–S113, doi: 10.1190/1.3555529.
Sun, R., G. A. McMechan, C.-S. Lee, J. Chow, and C.-H. Chen, 2006, Prestack scalar reverse-time depth migration of 3D elastic seismic data: Geophysics, **71**, no. 5, S199–S207, doi: 10.1190/1.2227519.
Thomsen, L., 1986, Weak elastic anisotropy: Geophysics, **51**, 1954–1966, doi: 10.1190/1.1442051.
Tsvankin, I., 2005, Seismic signatures and analysis of reflection data in anisotropic media, 2nd ed.: Elsevier.
Virieux, J., 1986, P-SV wave propagation in heterogeneous media: Velocity-stress finite-difference method: Geophysics, **51**, 889–901, doi: 10.1190/1.1442147.
Vyas, M., D. Nichols, and E. Mobley, 2011, Efficient RTM angle gathers using source directions: 81st Annual International Meeting, SEG, Expanded Abstracts, 3104–3108.
Xie, X., and R. S. Wu, 2002, Extracting angle domain information from migrated wavefields: 72nd Annual International Meeting, SEG, Expanded Abstracts, 1360–1363.
Xu, S., Y. Zhang, and B. Tang, 2011, 3D angle gathers from reverse time migration: Geophysics, **76**, no. 2, S77–S92, doi: 10.1190/1.3536527.
Xu, S., and H. Zhou, 2014, Accurate simulations of pure quasi-P-waves in complex anisotropic media: Geophysics, **79**, no. 6, T341–T348, doi: 10.1190/geo2014-0242.1.
Yan, J., and P. Sava, 2008, Isotropic angle-domain elastic reverse time migration: Geophysics, **73**, no. 6, S229–S239, doi: 10.1190/1.2981241.
Yan, J., and P. Sava, 2009a, 3D elastic wave mode separation for TTI media: 79th Annual International Meeting, SEG, Expanded Abstracts, 4294–4298.
Yan, J., and P. Sava, 2009b, Elastic wave-mode separation for VTI media: Geophysics, **74**, no. 5, WB19–WB32, doi: 10.1190/1.3184014.
Yan, J., and P. Sava, 2011, Improving the efficiency of elastic wave-mode separation for heterogeneous tilted transverse isotropic media: Geophysics, **76**, no. 4, T65–T78, doi: 10.1190/1.3581360.
Yoon, K., M. Guo, J. Cai, and B. Wang, 2011, 3D RTM angle gathers from source wave propagation direction and dip of reflector: 81st Annual International Meeting, SEG, Expanded Abstracts, 1057–1060.
Yoon, K., and K. J. Marfurt, 2006, Reverse-time migration using the Poynting vector: Exploration Geophysics, **37**, 102–107, doi: 10.1071/EG06102.
Zhang, Q., and G. A. McMechan, 2010, 2D and 3D elastic wavefield vector decomposition in the wavenumber domain for VTI media: Geophysics, **75**, no. 3, D13–D26, doi: 10.1190/1.3431045.